Journal of Alloys and Compounds 509 (2011) 2011–2015

Contents lists available at ScienceDirect

Journal of Alloys and Compounds

journal homepage: www.elsevier.com/locate/jallcom

Characterization of RuO_2 nanocrystals deposited on carbon nanotubes by reactive sputtering

Y.C. Su [a], C.A. Chen [a], Y.M. Chen [a], Y.S. Huang [a,*], K.Y. Lee [a,b], K.K. Tiong [c]

[a] Department of Electronic Engineering, National Taiwan University of Science and Technology, 43 Keelung Road, Section 4, Taipei 106, Taiwan
[b] Graduate Institute of Electro–Optical Engineering, National Taiwan University of Science and Technology, 43 Keelung Road, Section 4, Taipei 106, Taiwan
[c] Department of Electrical Engineering, National Taiwan Ocean University, Keelung 202, Taiwan

ARTICLE INFO

Article history:
Received 5 August 2010
Received in revised form 12 October 2010
Accepted 22 October 2010
Available online 3 November 2010

PACS:
61.46.−w
68.37.Lp
78.30.−j

Keywords:
Nanostructured materials
Oxide materials
RF magnetron sputtering
X-ray photoelectron spectroscopy
Scanning electron microscopy
Transmission electron microscopy
Raman scattering

ABSTRACT

We report deposition and characterization of RuO_2 nanocrystals (NCs) on carbon nanotubes (CNTs) by reactive radio frequency magnetron sputtering using a Ru target. Field-emission scanning electron microscopy micrographs showed the surface morphology of the as-deposited RuO_2 varied from nanoparticle-like to tube-like NCs as the oxygen flux increased from 2 to 10 sccm. X-ray diffraction pattern confirmed the formation of pure rutile RuO_2 NCs on CNTs. The transmission electron microscopy image of RuO_2-coated CNTs revealed that RuO_2 NCs had been deposited on the surface of the CNTs with uniform size distribution and random directions. X-ray photoelectron spectroscopy spectra indicated the coexistence of higher oxidation states of ruthenium in the as-deposited RuO_2 NCs. The red-shifts of the peak positions and broadening of linewidths of the Raman features were attributed to both the size and residual stress effects.

1. Introduction

Ruthenium oxide (RuO_2) is a well-known metallic oxide with important applications in catalysts and supercapacitors [1,2]. From the practical point of view, a porous composite structure with a well-controlled size and/or shape distribution of RuO_2 nanocrystals (NCs) is highly desirable in order to increase the surface-to-volume ratio. The large value of surface-to-volume ratio makes possible the high performance of devices [3]. Since the high-density carbon nanotubes (CNTs) provide ideal porous structures, developing RuO_2-coated CNTs nanocomposites is highly desirable [4–6]. Several techniques have been developed for fabricating RuO_2 nanostructures using CNTs as the template [7–9]. However, to date, there is very little work done on deposition of RuO_2 nanostructures on CNTs by reactive radio frequency magnetron sputtering (RFMS). The RFMS is a simple technique for fabricating large area structures, which has several advantages, including better control of the growth conditions and a single deposition step to obtain the nanostructures.

In this work, RuO_2 nanostructures were deposited onto the CNTs templates by RFMS using a Ru target under different conditions. The surface morphology, structural and spectroscopic properties of the as-deposited NCs were characterized using field-emission scanning electron microscopy (FESEM), X-ray diffraction (XRD), transmission electron microscopy (TEM), X-ray photoelectron spectroscopy (XPS) and micro-Raman spectroscopy. The results were presented and discussed.

2. Experimental

The study was performed using a home-made high vacuum RFMS system. The sputtering target was a 1-in. Ru (99.95%) metal. The CNT templates were synthesized onto p-type Si (1 0 0) substrates using thermal chemical vapor deposition [7]. Two separate gas lines, each equipped with a mass flow controller, were used to control the Ar and O_2 flow rates. The sample holder was approximately 45 mm from the target. The sputtering chamber was evacuated with a turbo-molecular pump and has a base pressure of $\sim 3 \times 10^{-5}$ mbar. The reactive sputtering was carried out in a mixture of argon (10 sccm) and oxygen (2–10 sccm) gases. O_2 was introduced over the substrate into the sputtering chamber with Ar atmosphere. The working pressure of 1.2×10^{-1} mbar, power of the RF generator at 50 W, substrate temperature T_s at 200 °C, and 10 or 120 min deposition time were used in the experiment.

* Corresponding author. Tel.: +886 2 27376385, fax: +886 2 27376424.
E-mail address: ysh@mail.ntust.edu.tw (Y.S. Huang).

0925-8388/$ – see front matter © 2010 Elsevier B.V. All rights reserved.
doi:10.1016/j.jallcom.2010.10.121

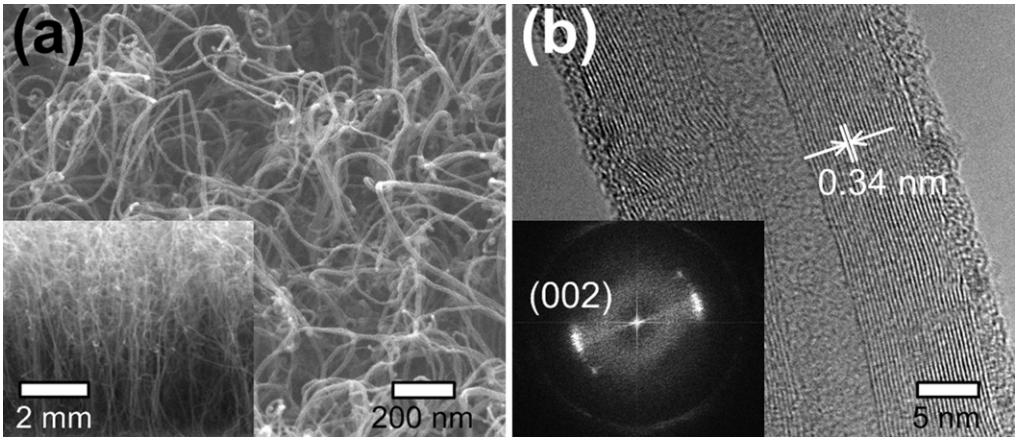

Fig. 1. (a) The SEM image of top view of the pristine CNTs; the inset shows cross-sectional view of CNTs. (b) The HRTEM image of the pristine CNT; the inset is the FFT pattern.

The morphology of the RuO_2 NCs on CNTs (denoted as RuO_2/CNT) was recorded using a JEOL-JSM6500F field-emission scanning electron microscope with an accelerating voltage of 15 kV. Crystal structures were analyzed using a Rigaku D/Max-RC X-ray diffractometer equipped with Cu Kα radiation source and Ni filter. TEM images were recorded to characterize the structure of RuO_2/CNT by a Phillips Tecnai G2 F20 FE-TEM at a working voltage of 200 kV. The chemical binding states of RuO_2 NCs were analyzed by XPS using a Thermo VG Scientific Theta Probe system under the base pressure of 1.3×10^{-7} Pa. The Al Kα 1486.68 eV line was used as the X-ray source. Before the measurement, the system was calibrated using the Ag $3d_{5/2}$ line at 368.26 eV. XPS peak positions and integrated intensities were obtained through the curve fitting, using Thermo VG Scientific: Avantage v2.13 Software. Raman spectra were recorded on a Renishaw inVia micro-Raman system with 1800 grooves/mm grating and an optical microscope with a 50× objective at room temperature. The Ar-ion laser beam of the 514.5 nm excitation line with a power of about 1 mW was focused on a spot size ~5 μm in diameter.

3. Results and discussion

Fig. 1(a) depicts the tilt-view SEM image taken from top of the pristine CNTs. The inset of Fig. 1(a) shows the cross-sectional view SEM image of CNTs revealing the vertically aligned CNTs with respect to the substrate surface. Fig. 1(b) is the high resolution TEM (HRTEM) image of a CNT revealing the multiwall nature of the pristine CNT. The HRTEM image indicates that the multiwall CNT has

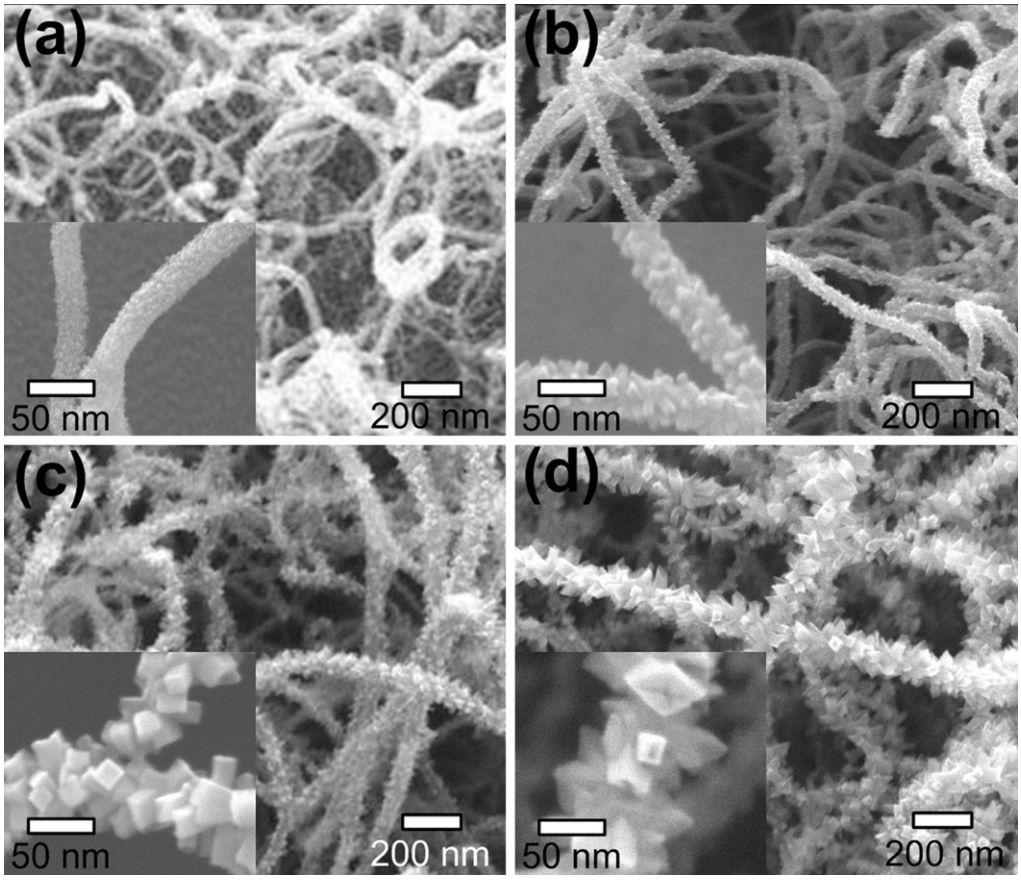

Fig. 2. The tilt-view SEM images of RuO_2/CNT nanocomposites with the oxygen fluxes of (a) 2, (b) 3, (c) 5, and (d) 10 sccm, respectively. The inserts are the enlarged images of the samples.

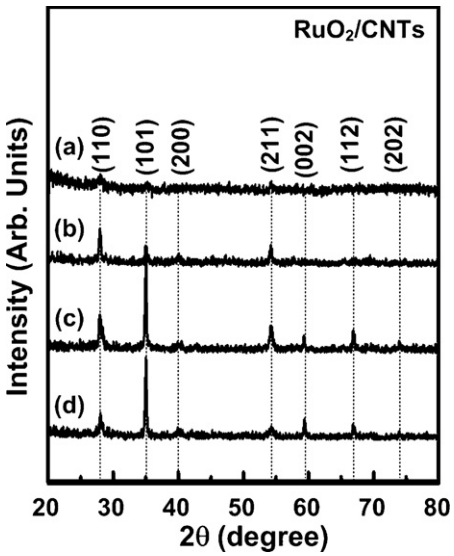

Fig. 3. The XRD pattern of RuO_2/CNT nanocomposites deposited under the oxygen fluxes of (a) 2, (b) 3, (c) 5, and (d) 10 sccm for 120 min.

clear graphite layers with defects parallel to the tube axis. The interlayer spacing is about 0.34 nm. The inset of Fig. 1(b) shows the fast fourier transform (FFT) analysis of the HRTEM image of the CNT. The FFT pattern exhibits a pair of small but strong arcs for (0 0 2) which indicates dominant (0 0 2) plane orientation of the CNTs [10]. Fig. 2(a)–(d) show the tilt-view SEM images of RuO_2/CNT with the oxygen fluxes of 2, 3, 5, and 10 sccm, respectively. The insets of Fig. 2(a)–(d) are the enlarged images of the corresponding samples. The FESEM images of the RuO_2/CNT nanocomposites in Fig. 2 clearly show CNTs with a larger tubular diameter near the tips due to the presence of the coating of RuO_2. During overhead sputtering deposition, the RuO_2 was directly coated on top of the CNT template; the coated tips shielded the lower parts of the tubes from being coated by the oxide. The enlarged images shown in Fig. 2 (see insets) indicate that the surface morphologies of the as-deposited RuO_2 NCs vary from nanoparticle-like to rod-like and tube-like NCs with increasing NC sizes as the oxygen flux increases from 2 to 10 sccm. The nanoparticle-like RuO_2 NCs can be used as a protective layer on CNTs, providing stable and uniform field emission [11]. While the nanotube-like structure can increase the surface-to-volume ratio which makes the RuO_2/CNT nanocomposites as attractive candidate for the supercapacitor applications. A preliminary study has been carried out to investigate the potential application of

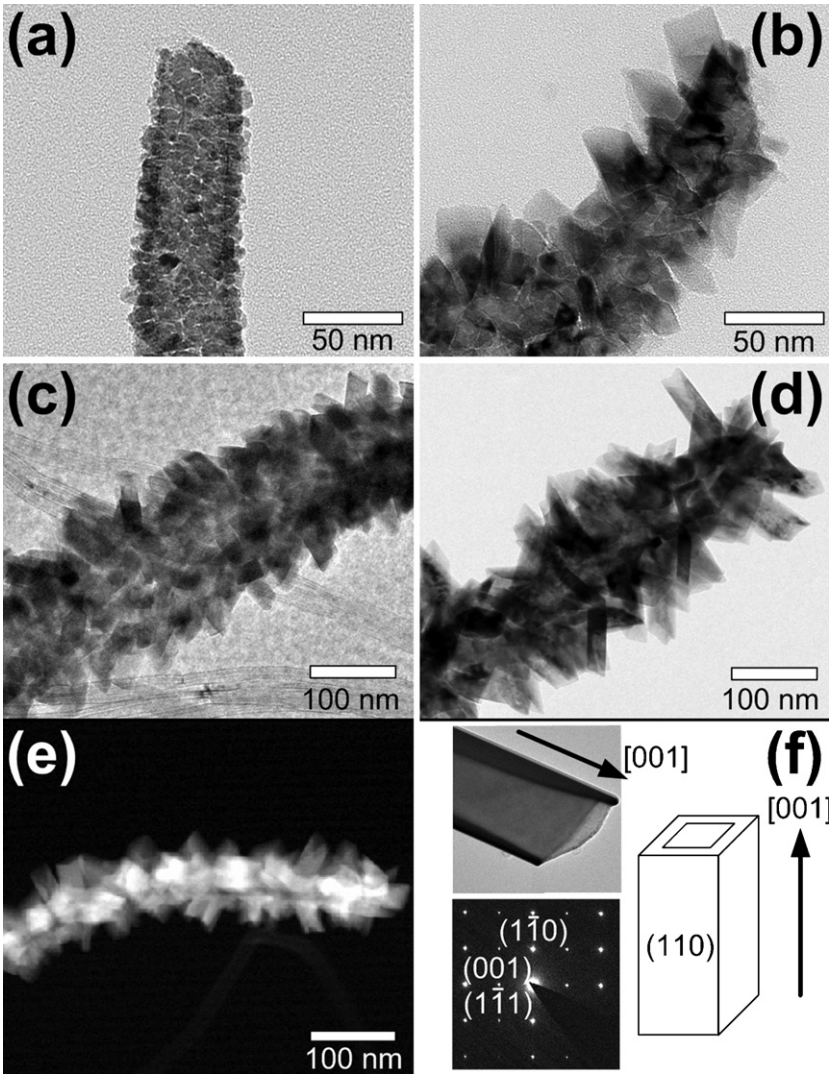

Fig. 4. The TEM images of RuO_2/CNT nanocomposites deposited under oxygen fluxes of (a) 2, (b) 3, (c) 5, and (d) 10 sccm, respectively. (e) The HAADF image of RuO_2 nanotubes on CNT. (f) Upper part of left-hand side: TEM image focused on a RuO_2 nanotube; lower part of left-hand side: the SAED pattern taken from the tube side wall; right-hand side: a schematic of the tubular crystal of RuO_2.

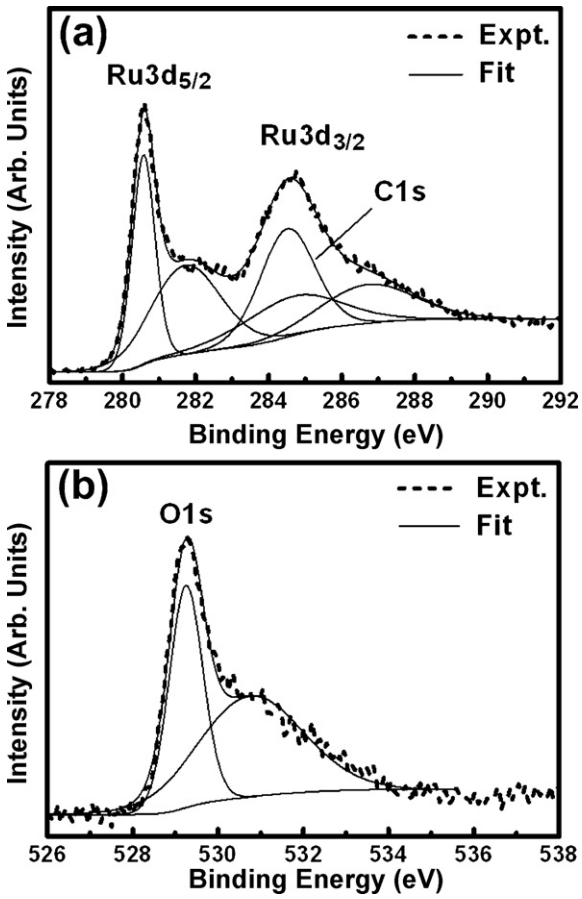

Fig. 5. Experimental and fitted XPS spectra in the vicinity of (a) Ru 3d and (b) O 1s core-electron lines obtained from the RuO_2/CNT nanocomposites.

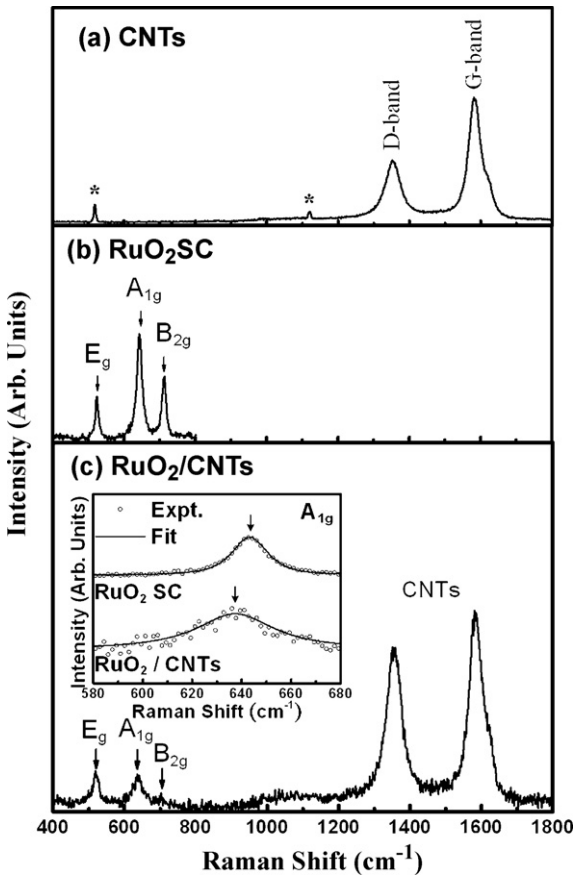

Fig. 6. Raman spectra of (a) CNTs, (b) RuO_2 SC, and (c) RuO_2/CNT nanocomposites.

nanotube-like RuO_2/CNT nanocomposites as electrode materials in electrochemical capacitors [12]. The average specific capacitance obtained for the nanotube-like RuO_2/CNT nanocomposites is about 140 F/g, which is much larger than that of the pure CNTs (30 F/g). The enhancement of the specific capacitance can be attributed to the presence of RuO_2 on the surface of CNTs, which modifies the structure and morphology of CNTs, allowing the RuO_2 to be available for the electrochemical reactions and improves the efficiency of the nanocomposites. The progressive redox reactions occurring at the surface and bulk of RuO_2 through faradiac charge transfer between electrolyte and electrode results in the enhancement of the specific capacitance of RuO_2/CNT nanocomposites from pure CNTs.

Fig. 3 shows the XRD pattern of RuO_2/CNT nanocomposites deposited under the oxygen fluxes of 2, 3, 5, and 10 sccm for 120 min. The presence of rutile structure of RuO_2 in the nanocomposites is confirmed by the main characteristic diffraction peaks of the RuO_2 (1 1 0), (1 0 1), (2 1 1) and (0 0 2) planes at 2θ values of around 28°, 35°, 54°, and 59°, respectively. The intensities and linewidths of XRD features for the nanocomposites deposited under the oxygen flux of 2 sccm are weaker and broader as compared with that deposited under 10 sccm. The weaker intensity and broadening of linewidth can be attributed to the smaller sizes of the as-deposited nanoparticles under the oxygen flux of 2 sccm. As shown in Fig. 3, the relative intensities of the main features vary with oxygen flux. For example, the largest intensity of the XRD spectra changes from (1 1 0) to (1 0 1) plane when the oxygen flux increases from 3 to 5 sccm. The XRD spectrum for the sample deposited under the oxygen flux of 10 sccm indicates that the most preferred orientations are (1 1 0), (1 0 1) and (0 0 2) planes with the intensity of (1 0 1) plane I_{101} to be the largest ($I_{101} > I_{110} \approx I_{002}$). The results are different from that of the RuO_2 standard listed in JCPDS 88-0322 where the three most preferred orientations are (1 1 0), (1 0 1) and (2 1 1) planes with $I_{110} > I_{101} > I_{211}$.

TEM investigations were carried out for a more detailed structural characterization. Fig. 4(a)–(d) are the TEM images of RuO_2/CNT nanocomposites deposited under oxygen fluxes of 2, 3, 5 and 10 sccm, respectively. As shown in Fig. 4(a)–(c), the TEM images of RuO_2/CNT nanocomposites reveal that uniform size distribution and random directions of RuO_2 NCs were deposited onto the CNT. The sizes of RuO_2 are about 5–20 nm and increased with increasing oxygen flux. When the oxygen flux is increased to 10 sccm, as can be seen in Fig. 4(d), the distinct nanotube-like of the RuO_2 NCs were deposited onto the surface of CNT. Fig. 4(e) is the high angle annular dark-field (HAADF) image of RuO_2 nanotubes on a CNT. The HAADF image indicates that the center portion still retains a tubular structure after depositing RuO_2 NCs. Energy-dispersive X-ray spectroscopy measurements reveal that the NCs have an average atomic ratio of Ru to O of 1:2. The upper left hand part of Fig. 4(f) shows the TEM image focused on a RuO_2 nanotube deposited on CNTs. The lower left hand part of Fig. 4(f) is the selected-area electron diffraction (SAED) pattern taken from the tube side wall. The SAED pattern has been identified to be the [1 1 0] zone pattern, indicating that the tube walls belong to the {1 1 0} facets and the preferential growth direction of the RuO_2 nanotube is along the [0 0 1] direction. A schematic of tubular RuO_2 NCs is illustrated on the right hand side of Fig. 4(f).

XPS is frequently used as a complementary technique for assigning oxidation states and the stoichiometry of the oxides. A slow scan XPS was performed on Ru 3d doublet (5/2 and 3/2) and oxygen O 1s peaks in the binding energy ranges of 278–292 eV and 526–536 eV,

respectively. Fig. 5 shows the peak fitted slow scan XPS spectra of (a) Ru 3d and (b) O 1s core-electron peaks obtained from the RuO_2/CNT nanocomposites deposited under oxygen flux of 10 sccm. C 1s peak which appears at ~284 eV can overlap with Ru^{4+} $3d_{3/2}$ or its satellite peak. Besides the C 1s feature located at ~284 eV, the Ru 3d signal of NCs shows two different binding states of ruthenium atoms and exhibit asymmetric line shapes. These two peaks are identified to be the 4+ oxidation states of Ru $3d_{5/2}$ and $3d_{3/2}$ at ~280.6 eV and ~284.7 eV, respectively. The location of the peaks of 4+ oxidation states of Ru are close to those of the single crystal at 281.1 eV and 285.1 eV, respectively [13]. Quantitative deconvolution of the XPS spectra revealed two additional features with broader character at ~281.7 eV and ~286.7 eV, respectively, for the Ru $3d_{5/2}$ and $3d_{3/2}$ regions and are higher than the major peaks by ~1.1 and ~2.0 eV, respectively. The XPS results of O 1s peak show doublet signals with broader satellite at higher binding energy situated at ~530.8 eV. The major peak position at ~529.3 eV is similar to that of O 1s of the RuO_2 single crystal and corresponding to oxygen in the metal–O–metal bond [13]. We have tentatively assigned these broader extra features located at higher binding energy sites of Ru 3d and O 1s to the existence of an impurity of higher oxidation states in the RuO_2 NCs.

Fig. 6(a)–(c) shows the Raman spectra of the CNTs, RuO_2 single crystal (SC), and RuO_2/CNT nanocomposites, respectively. Raman signals from the Si substrate are marked by an asterisk. The spectrum of the CNTs (Fig. 6(a)) shows a D-band at ~1355 cm^{-1} originating from the disordered carbon and a G-band at ~1586 cm^{-1} corresponding to sp^2-hybridized carbon [14]. The Raman spectrum of RuO_2 SC (see Fig. 6(b)), shows three Raman modes: E_g at 528 cm^{-1}, A_{1g} at 646 cm^{-1} and B_{2g} at 716 cm^{-1}. Fig. 6(c) is the Raman spectrum of the RuO_2/CNT nanocomposites with oxygen flux of 2 sccm, which reveals three RuO_2 features (E_g at 518 cm^{-1}, A_{1g} at 634 cm^{-1} and B_{2g} at 693 cm^{-1}) and two CNTs signatures (D-band at ~1349 cm^{-1}, and G-band at ~1579 cm^{-1}). The red-shifts in the peak positions and linewidth broadening for the RuO_2 features (see inset) can be attributed to both the size and residual stress effects [15].

4. Summary

RuO_2 NCs were deposited on CNT templates by reactive RFMS using a Ru target under different mixture of argon and oxygen fluxes. FESEM micrographs showed that the surface morphology of the as-deposited RuO_2 varied from nanoparticle-like to tube-like NCs as the oxygen fluxes increased from 2 to 10 sccm. The nanoparticles-like RuO_2 NCs can be used as a protective layer on CNTs, which have applications in providing stable and uniform field emission. The nanotube-like structure can increase the surface-to-volume ratio which makes the RuO_2/CNT nanocomposites as attractive candidate for the supercapacitor applications. XRD pattern confirmed the formation of pure rutile RuO_2 NCs on CNTs. The TEM image of RuO_2-coated CNT revealed that RuO_2 NCs had been deposited on the surface of the CNT with uniform size distribution and random directions. XPS spectra showed the coexistence of higher oxidation states of ruthenium in the as-deposited RuO_2 NCs. The red-shifts of the peak positions and broadening of linewidths of the RuO_2 Raman features were attributed to both the size and residual stress effects.

Acknowledgments

This work is financial supported by the National Science Council of Taiwan under project nos. NSC-97-2112-M-011-001-MY3, NSC-97-2221-E-011-017 and NSC-98-2221-E-011-021.

References

[1] H. Yu, K. Zeng, X. Fu, Y. Zhang, F. Peng, H. Wang, J. Yang, J. Phys. Chem. C 112 (2008) 11875–11880.
[2] Y.F. Ke, D.S. Tsai, Y.S. Huang, J. Mater. Chem. 15 (2005) 2122–2127.
[3] J.V. Ryan, A.D. Berry, M.L. Anderson, J.W. Long, R.M. Stroud, V.M. Cepak, V.M. Browning, R.D. Rolison, C.I. Merzbacher, Nature (London) 406 (2000) 169–172.
[4] W.C. Fang, O. Chyan, C.L. Sun, C.T. Wu, C.P. Chen, K.H. Chen, L.C. Chen, J.H. Huang, Electrochem. Commun. (2007) 239–244.
[5] (a) J.G. Zhou, H.T. Fang, Y.F. Hu, T.K. Sham, C.X. Wu, M. Liu, F. Li, J. Phys. Chem. C 113 (2009) 10747–10750;
(b) R.R. Bi, X.L. Wu, F.F. Cao, L.Y. Jiang, Y.G. Guo, L.J. Wan, J. Phys. Chem. C 114 (2010) 2448–2451.
[6] Y.J. Gu, W.T. Wong, J. Clust. Sci. 17 (2006) 517–526.
[7] H.B. Lian, K.Y. Lee, K.Y. Chen, Y.S. Huang, Diam. Relat. Mater. 18 (2009) 541–543.
[8] J.S. Ye, H.F. Cui, X. Liu, T.M. Lim, W.D. Zhang, F.S. Sheu, Small 1 (2005) 560–565.
[9] Z. Sun, Z. Liu, B. Han, S. Miao, J. Du, Z. Miao, Carbon 44 (2006) 888–893.
[10] T. Kyotani, L.F. Tsai, A. Tinuta, Chem. Mater. 8 (1996) 2109–2113.
[11] C.A. Chen, K.Y. Lee, Y.M. Chen, J.G. Chi, S.S. Lin, Y.S. Huang, Vacuum 84 (2010) 1427–1429.
[12] Y.C. Su, Master Thesis, National Taiwan University of Science and Technology, Taipei, Taiwan, 2010.
[13] A. Korotcov, H.P. Hsu, Y.S. Huang, D.S. Tsai, K.K. Tiong, Cryst. Growth Des. 6 (2006) 2501–2506.
[14] W.S. Bacsa, D. Ugarte, A. Châtelain, W.A. de Heer, Phys. Rev. B 50 (1994) 15473–15476.
[15] A. Korotcov, Y.S. Huang, K.K. Tiong, D.S. Tsai, J. Raman Spectrosc. 38 (2007) 737–749.